Electronic Supplementary Material (ESI) for Nanoscale.

In situ assembly of one-dimensional Pt@ZnO nanofibers driven by ZIF-8 framework for high-performance acetone sensor

Zaiping Chen, Wei Liu, Xiaohui Si, Junmeng Guo, Jiahang Huo, Zhiheng Zhang, Gang Cheng*, Zuliang Du*

Key Lab for Special Functional Materials, Ministry of Education, National & Local Joint Engineering Research Center for High-efficiency Display and Lighting Technology, School of Materials Science and Engineering, and Collaborative Innovation Center of Nano Functional Materials and Applications, Henan University, Kaifeng 475004, China

Email: weil@henu.edu.cn; chenggang@henu.edu.cn;

Characterization

The surface morphology of the samples was observed using a JEOL JSM-7610F Plus Scanning Electron Microscope (SEM) at an accelerating voltage of 5 kV. The prepared samples were analyzed by scanning transmission electron microscopy (STEM) and high-resolution TEM (HRTEM) images using a JEOL JEM-F200 transmission electron microscope (TEM) equipped with an energy dispersive X-ray spectrometer (EDX) at an operating voltage of 200 kV. The Brunauer, Emmett and Teller (BET) of the sample was determined by measuring the N_2 adsorption-desorption isotherms at 77.3K using the ASAP 2460 3.01 instrument. The photoluminescence (PL) spectra of the samples were measured using a fluorescence spectrometer (Edinburgh FLS1000, LTD., UK). Ultraviolet-visible absorption (UV-vis) spectroscopy was recorded by a UV-vis spectrophotometer (UV-1700). The samples were analyzed by X-ray powder diffraction (XRD) on a DX-2700B ray diffractometer using a metal body ceramic insulated Cu target radiation source (λ=1.54184 Å). X-ray photoelectron spectroscopy (XPS) spectra were obtained by using a Thermo Scientific K-Alpha system equipped with monochromatic Al Kα radiation (photon energy=1486.6 eV), whose typical parameter settings are: the step size is 0.1 eV, the constant analyzer energy is 50 eV over 5 sweeps, the spot size is 400 μm, the working voltage is 12 kV, the filament current is 6 mA, and the vacuum degree of the analysis chamber is better than 5.0E-7mBar. Background subtraction was made by the use of the Shirley algorithm with the end points chosen by averaging over 5 data points and all binding energies were referenced to the C 1s peak at 284.8 eV of surface adventitious carbon to correct for shifts caused by charge effects.[1] Peak fitting was done using the χ^2 minimization routine and optimization by Newton's method, as implemented in the XPSPEAK software.[2] The gas sensing properties were measured in WS-30B sensing system (Weisheng Instruments Co., Zhengzhou, China).

Methods of controlling humidity

The saturated water vapor pressure of a brine, which is directly proportional to the chemical activity of H_2O in the solution, will always be lower than the saturated water vapor pressure of pure water at the same temperature and total pressure. Thus, we control the relative humidity in the test chamber by configuring a saturated salt solution.[3] All sensors were first placed inside the testing chamber with a specific relative humidity generated by different saturated salt solutions (40% RH by using K_2CO_3, 55% RH by using NaBr, and 75% RH by using NaCl) in their equilibrium states.[4]

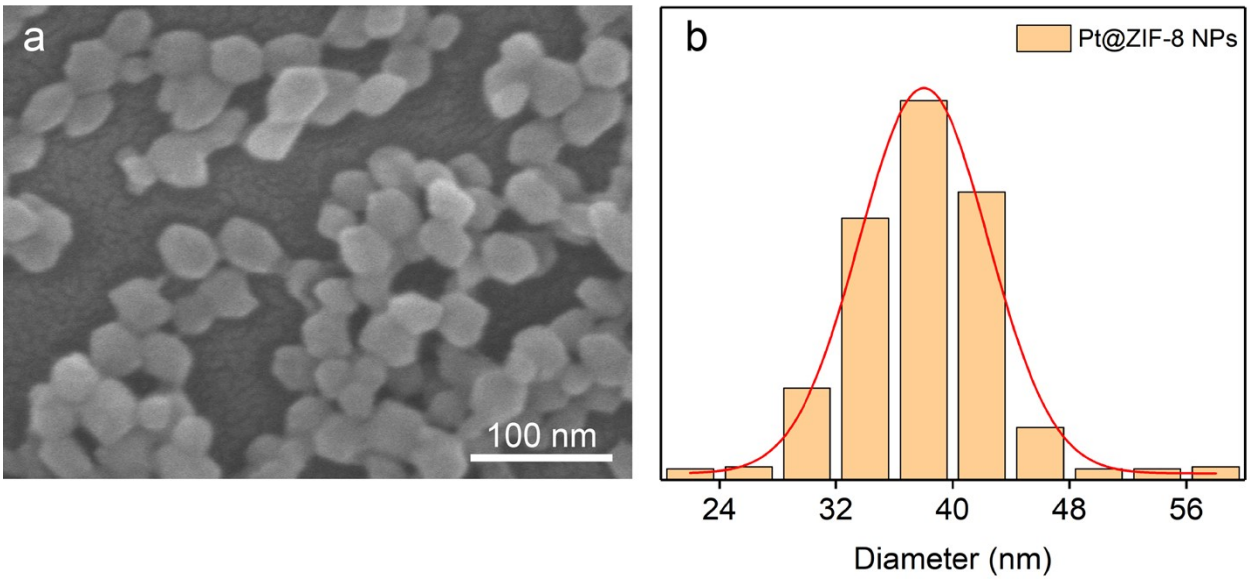

Figure S1. (a) SEM image and (b) size distribution histogram of Pt@ZIF-8 NPs.

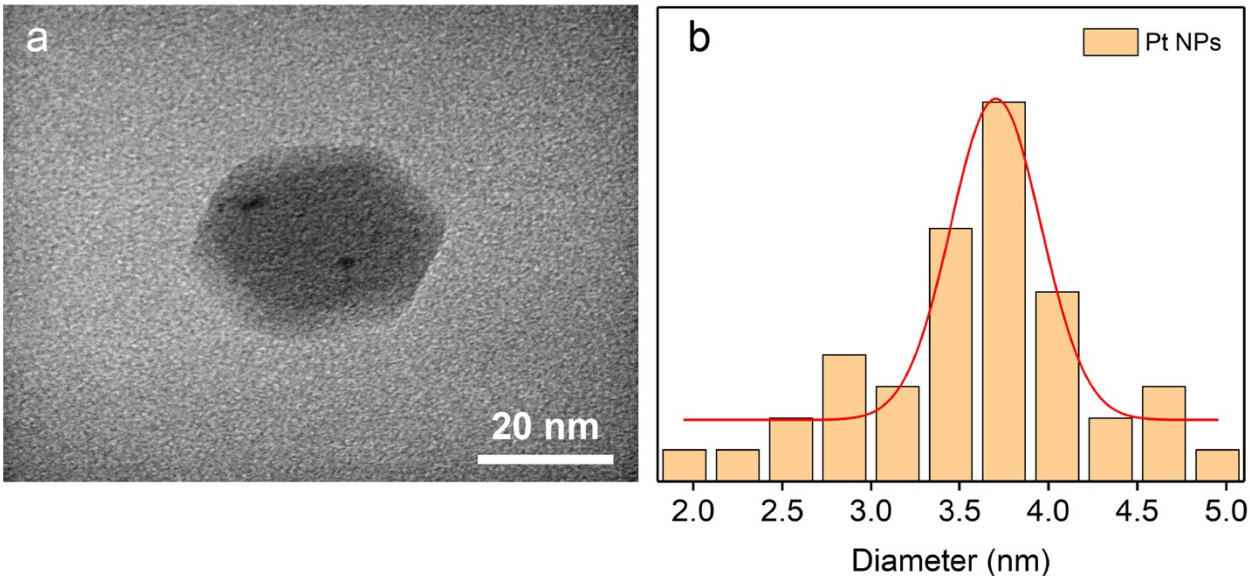

Figure S2. (a) TEM image and (b) size distribution histogram of Pt NPs.

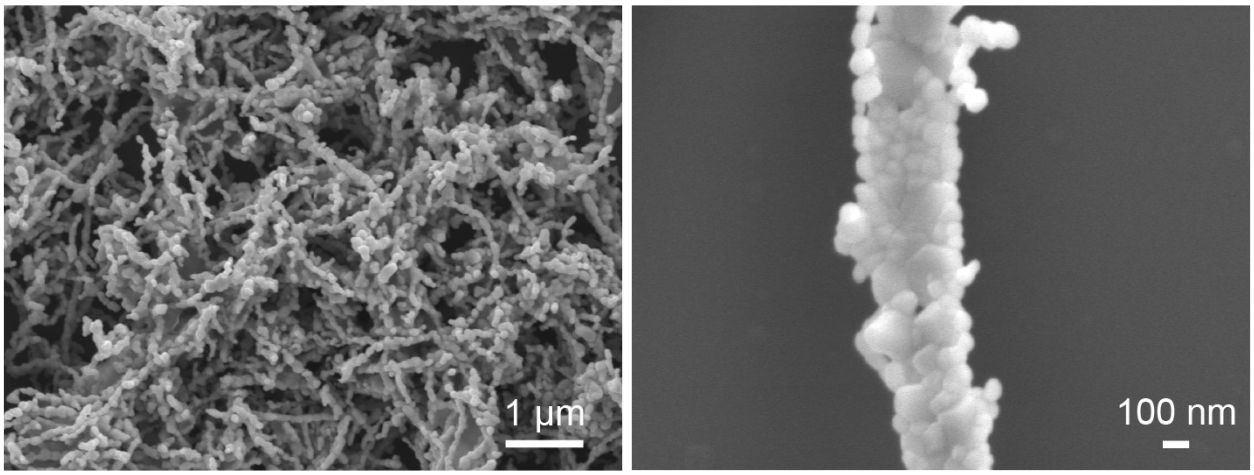

Figure S3. SEM images of ZnO NFs prepared without ZIF-8 framework.

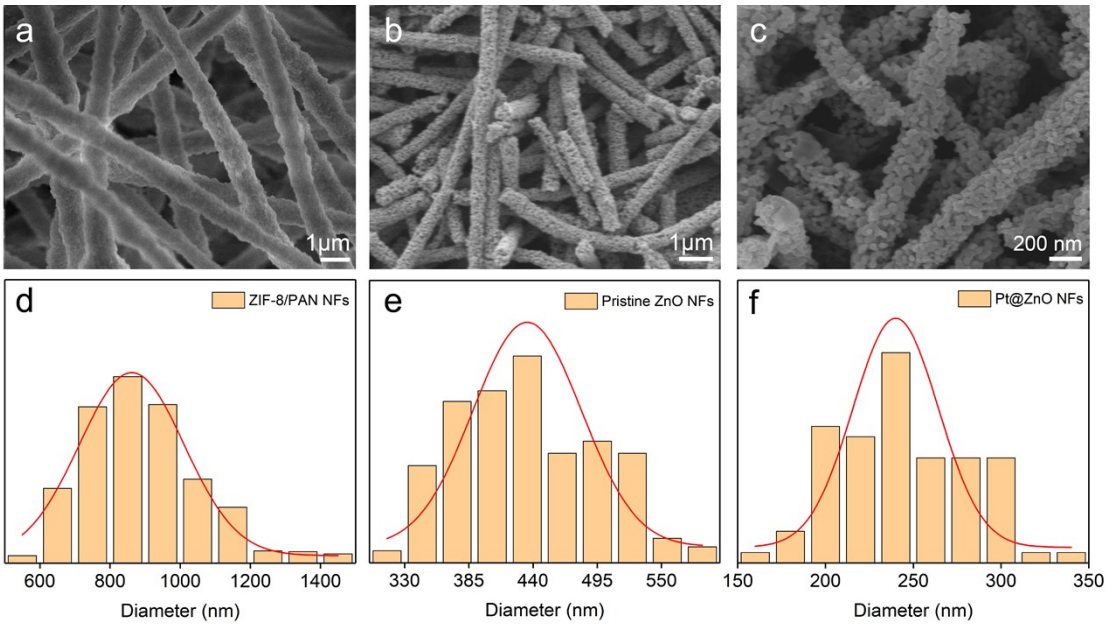

Figure S4. SEM images of (a) ZIF-8/PAN NFs, (b) pristine ZnO NFs and (c) Pt@ZnO NFs. Size distribution histograms of (d) ZIF-8/PAN NFs, (e) pristine ZnO NFs and (f) Pt@ZnO NFs.

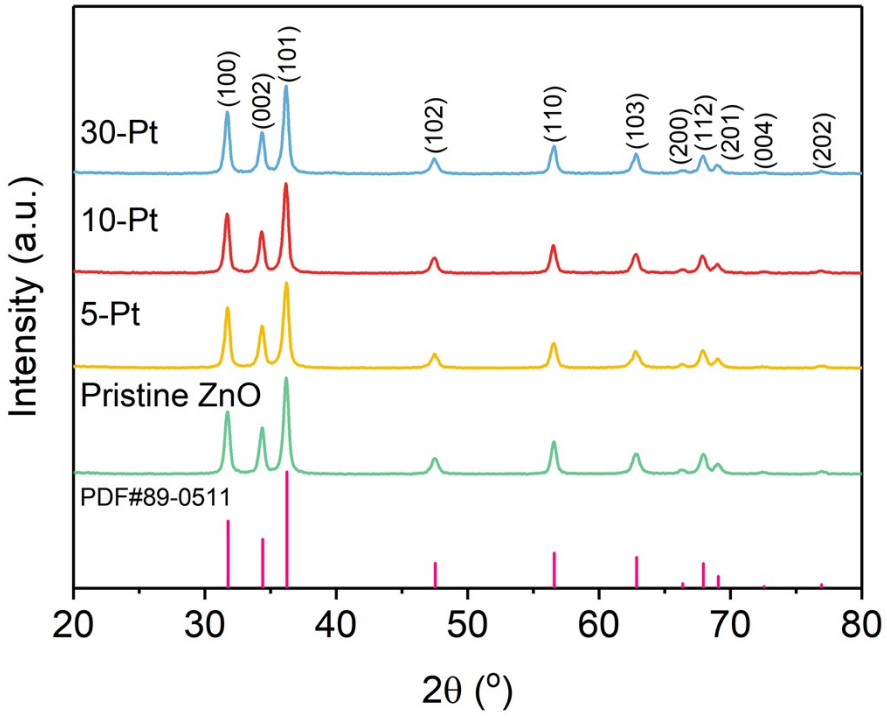

Figure S5. XRD images of pristine ZnO, 5-Pt, 10-Pt and 30-Pt.

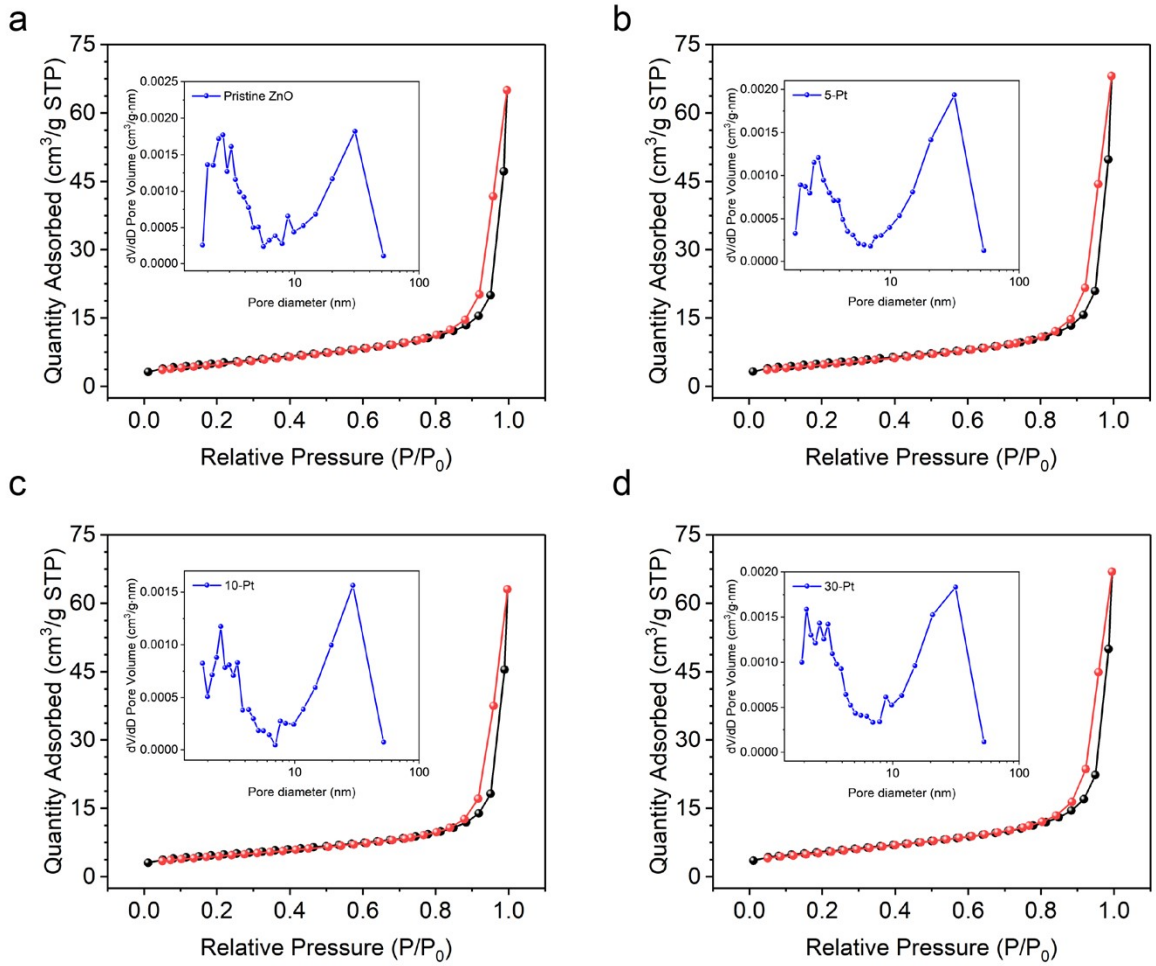

Figure S6. The typical N_2 adsorption-desorption isotherms and the corresponding pore size distribution curves (inset) of (a) pristine ZnO, (b) 5-Pt, (c) 10-Pt and (d) 30-Pt.

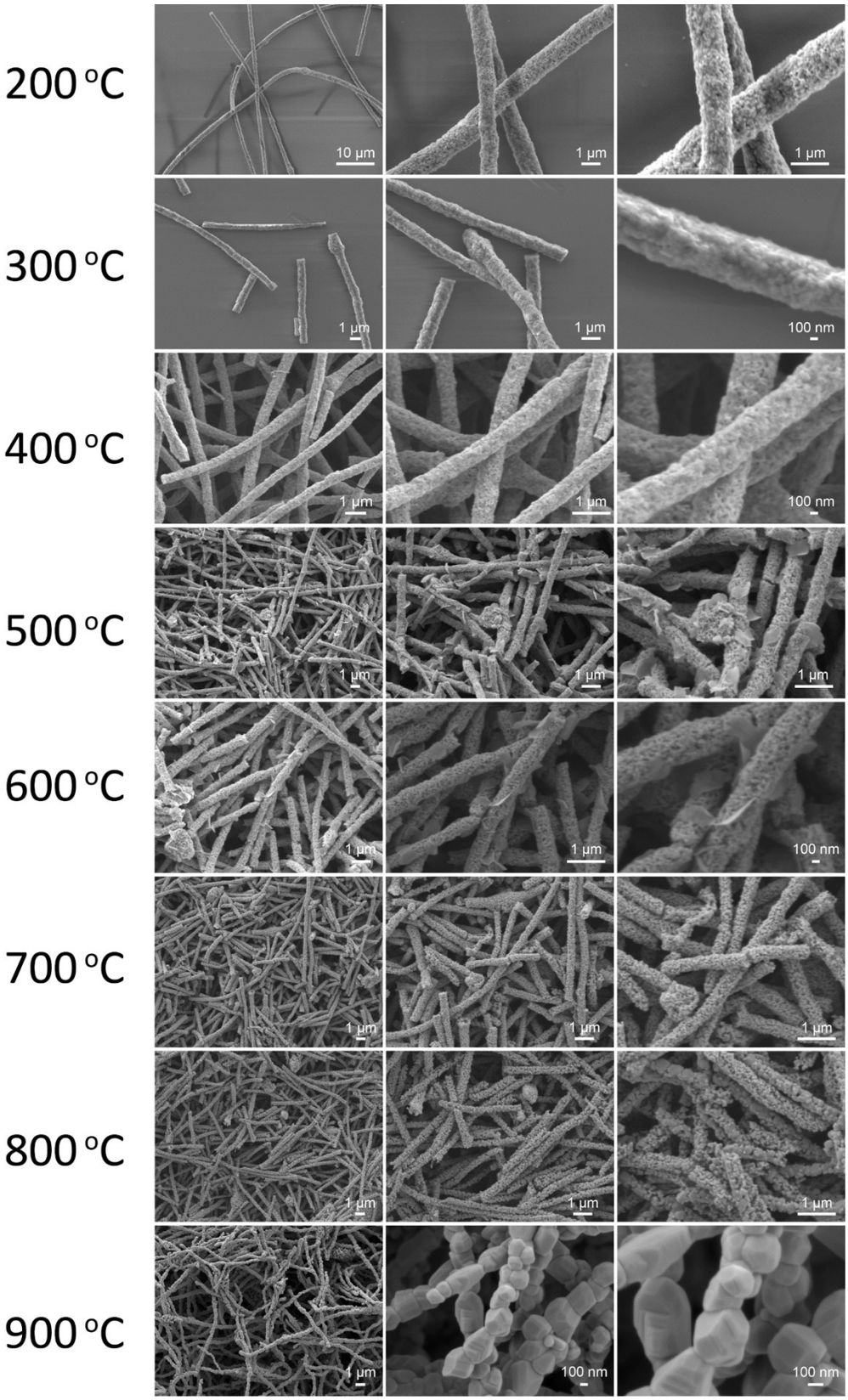

Figure S7. SEM images of Pt@ZnO NFs at annealing temperatures of 200 °C - 900 °C.

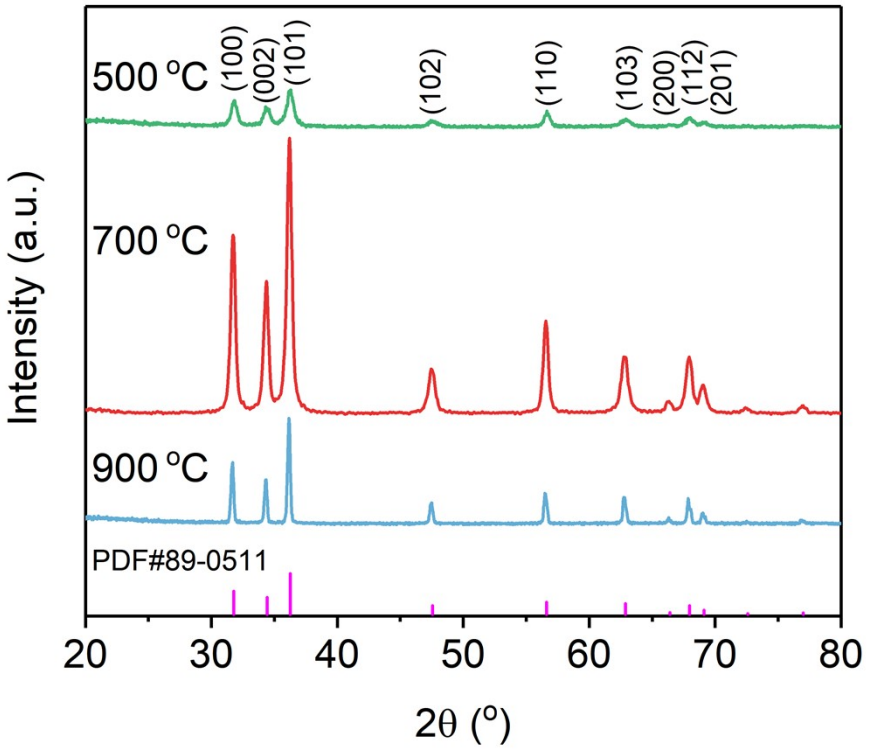

Figure S8. XRD images of Pt@ZnO NFs at annealing temperatures of 500 °C, 700 °C and 900 °C.

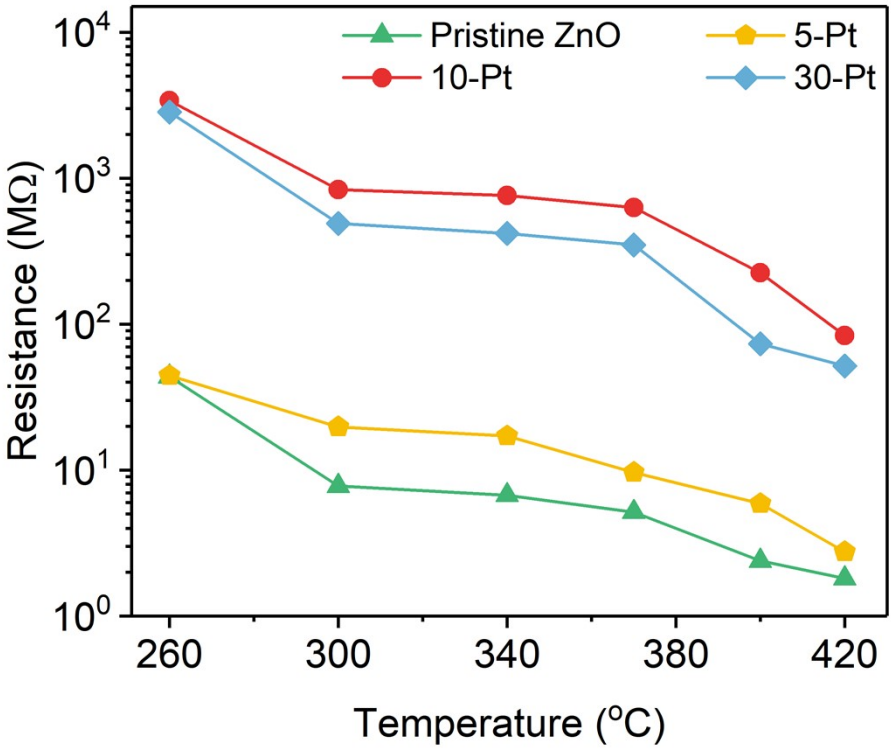

Figure S9. The variation of R_a with different operating temperature of pristine ZnO, 5-Pt, 10-Pt and 30-Pt sensors.

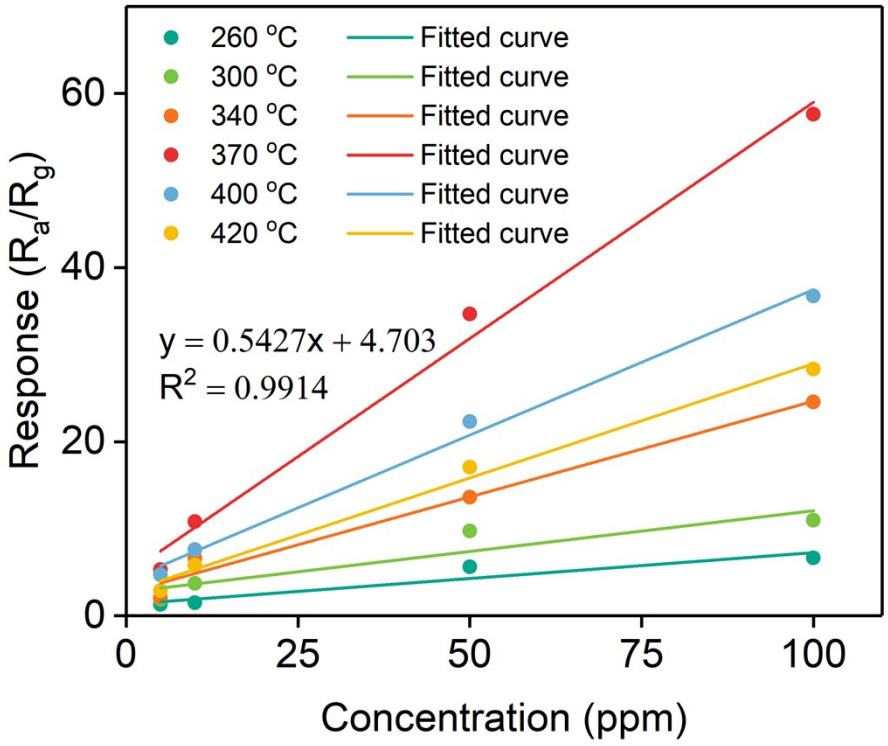

Figure S10. The response of 10-Pt sensor to different acetone concentrations at 260 °C - 370 °C.

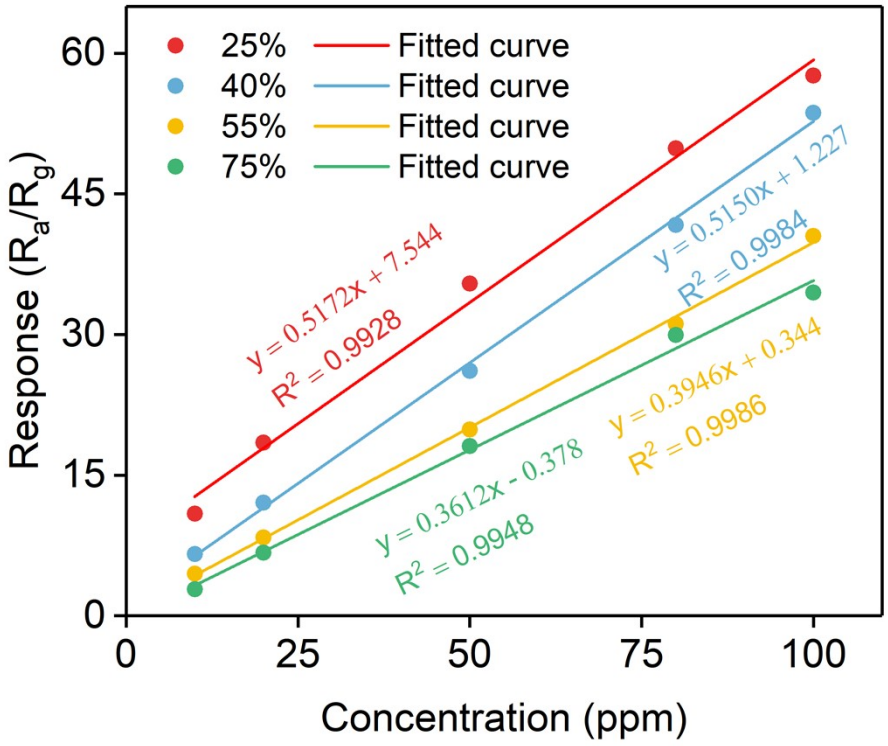

Figure S11. The response of 10-Pt sensor to different acetone concentrations at a RH range from 25% to 75%.

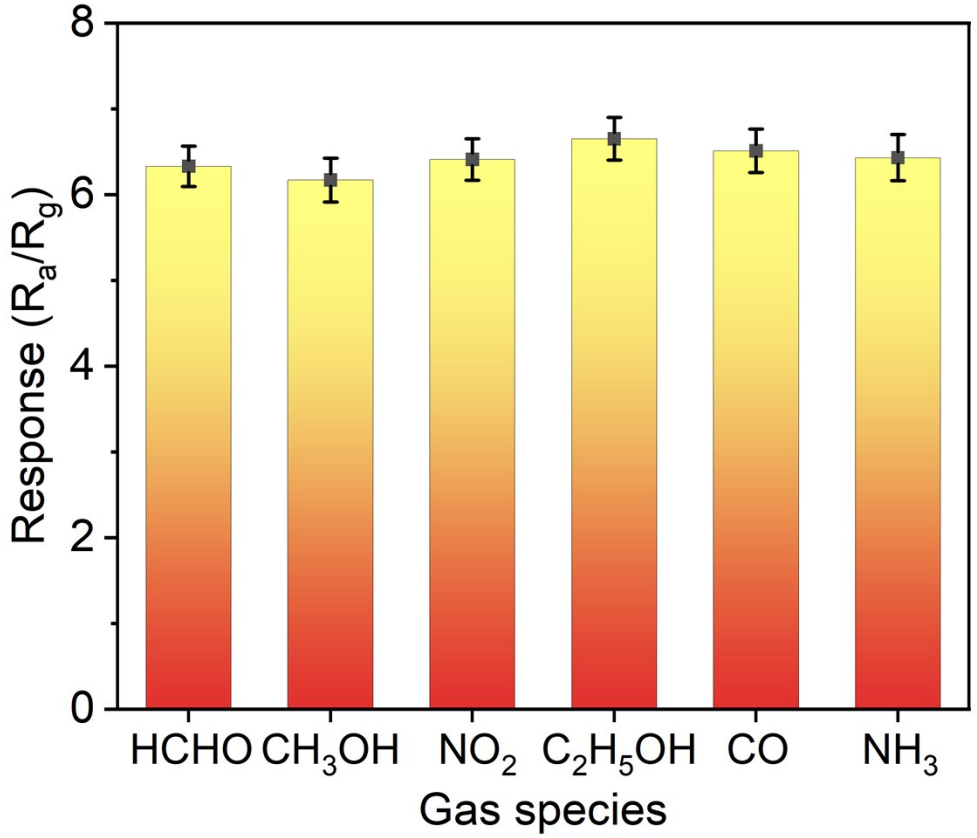

Figure S12. Cross-selectivity test of the 10-Pt sensor with 5 ppm interfering gases in the presence of 5 ppm acetone.

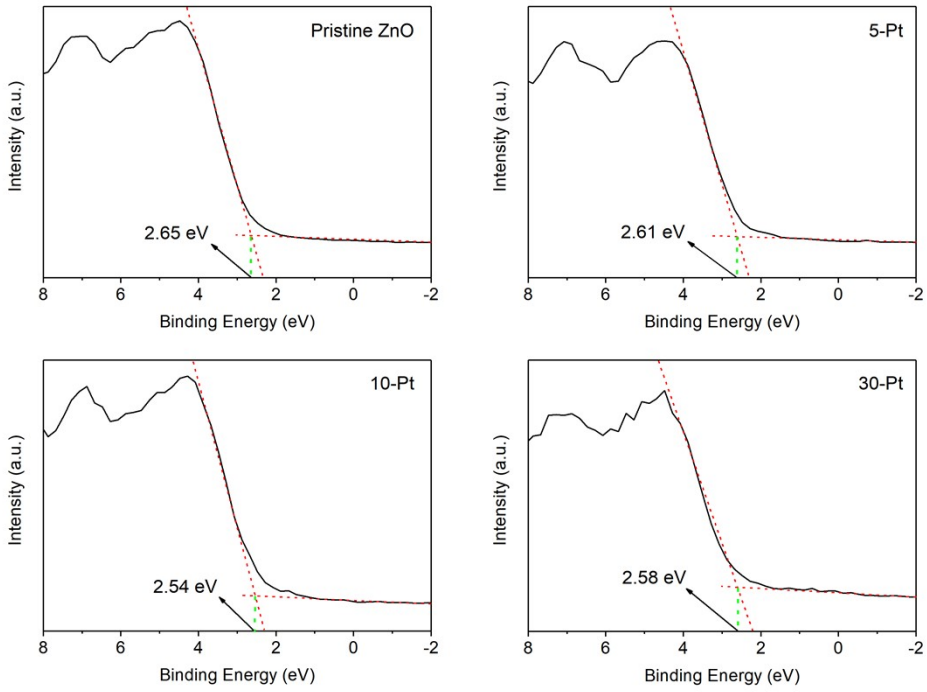

Figure S13. XPS valence band spectra of pristine ZnO, 5-Pt, 10-Pt and 30-Pt.

Table S1. Summary the cross-selectivity test of the 10-Pt sensor with interfering gases.

Gas species	Response of 10-Pt sensor
5 ppm acetone	6.12
5 ppm acetone + 5 ppm formaldehyde	6.33
5 ppm acetone + 5 ppm methanol	6.17
5 ppm acetone + 5 ppm nitrogen dioxide	6.41
5 ppm acetone + 5 ppm ethanol	6.65
5 ppm acetone + 5 ppm carbon monoxide	6.51
5 ppm acetone + 5 ppm ammonia	6.43

Table S2. Comparison of gas-sensing performances of various acetone sensors based on SMOs.

Materials	Working temperature (°C)	Concentration (ppm)	Response	Reference
Rutile TiO_2 Nanorods	320	100	12.3	[5]
ZnO/NPC	350	100	25.47	[6]
WO_3-C_3N_4 Nanosheet	340	100	35	[7]
La_2O_3-WO_3 Nanofibers	350	100	12.7	[8]
Au@ZnO Nanoplates	400	100	32	[9]
Co-doped ZnO Nanofibers	360	100	16	[10]
GO-WO_3 Nanofibers	375	100	35.9	[11]
α-MoO_3@NiO Nanocomposite	350	100	20.3	[12]
NiO/ZnO Hetrostructures	400	100	10	[13]
Au/SnO_2 Microstructures	340	100	18	[14]
TiO_2/SiC Heterojunctions	450	100	19.2	[15]
Pt@ZnO Nanofibers	370	100	57.61	This work

Reference

1. P. Swift, *Surface and Interface Analysis*, 1982, **4**, 47-51.
2. Y. C. G. Kwan, G. M. Ng and C. H. A. Huan, *Thin Solid Films*, 2015, **590**, 40-48.
3. Kinsman D J J. Evaporites, *Journal of Sedimentary Research*, 1976, **46**, 273-279.
4. T. D. Hong, R. H. Ellis, J. Gunn, D. Moore, *Journal of Stored Products Research*, 2002, **38**, 33-41.
5. S. Cao, N. Sui, P. Zhang, T. Zhou, J. Tu and T. Zhang, *J Colloid Interface Sci*, 2022, **607**, 357-366.
6. X. Chang, K. Li, X. Qiao, Y. Xiong, F. Xia and Q. Xue, *Sensors and Actuators B: Chemical*, 2021, **330**, 129366.
7. D. Wang, S. Huang, H. Li, A. Chen, P. Wang, J. Yang, X. Wang and J. Yang, *Sensors and Actuators B: Chemical*, 2019, **282**, 961-971.
8. C. Feng, C. Wang, P. Cheng, X. Li, B. Wang, Y. Guan, J. Ma, H. Zhang, Y. Sun, P. Sun, J. Zheng and G. Lu, *Sensors and Actuators B: Chemical*, 2015, **221**, 434-442.
9. Z. Feng, Y. Ma, V. Natarajan, Q. Zhao, X. Ma and J. Zhan, *Sensors and Actuators B: Chemical*, 2018, **255**, 884-890.
10. L. Liu, S. Li, J. Zhuang, L. Wang, J. Zhang, H. Li, Z. Liu, Y. Han, X. Jiang and P. Zhang, *Sensors and Actuators B: Chemical*, 2011, **155**, 782-788.
11. J. Zhang, H. Lu, C. Yan, Z. Yang, G. Zhu, J. Gao, F. Yin and C. Wang, *Sensors and Actuators B: Chemical*, 2018, **264**, 128-138.
12. K. Xu, S. Duan, Q. Tang, Q. Zhu, W. Zhao, X. Yu, Y. Yang, T. Yu and C. Yuan, *CrystEngComm*, 2019, **21**, 5834-5844.
13. N. Kaur, D. Zappa, M. Ferroni, N. Poli, M. Campanini, R. Negrea and E. Comini, *Sensors and Actuators B: Chemical*, 2018, **262**, 477-485.
14. J. Guo, J. Zhang, H. Gong, D. Ju and B. Cao, *Sensors and Actuators B: Chemical*, 2016, **226**, 266-272.
15. B. Wang, L. Deng, L. Sun, Y. Lei, N. Wu and Y. Wang, *Sensors and Actuators B: Chemical*, 2018, **276**, 57-64.